

Control, bi-stability and preference for chaos in time-dependent vaccination campaign

Enrique C. Gabrick,^{1,2,3, a)} Eduardo L. Brugnago,⁴ Ana L. R. de Moraes,⁵ Paulo R. Protachevicz,⁴ Sidney T. da Silva,⁶ Fernando S. Borges,^{3,7,8} Iberê L. Caldas,⁴ Antonio M. Batista,^{3,4,9} and Jürgen Kurths^{1,2}

¹⁾ *Potsdam Institute for Climate Impact Research, Telegrafenberg A31, 14473 Potsdam, Germany.*

²⁾ *Department of Physics, Humboldt University Berlin, Newtonstraße 15, 12489 Berlin, Germany.*

³⁾ *Graduate Program in Science, State University of Ponta Grossa, 84030-900, Ponta Grossa, PR, Brazil.*

⁴⁾ *Institute of Physics, University of São Paulo, 05508-090, São Paulo, SP, Brazil.*

⁵⁾ *Department of Physics, State University of Ponta Grossa, 84030-900, Ponta Grossa, PR, Brazil.*

⁶⁾ *Department of Chemistry, Federal University of Paraná, 81531-980, Curitiba, PR, Brazil.*

⁷⁾ *Department of Physiology and Pharmacology, State University of New York Downstate Health Sciences University, 11203, Brooklyn, New York, USA.*

⁸⁾ *Center for Mathematics, Computation, and Cognition, Federal University of ABC, 09606-045 São Bernardo do Campo, SP, Brazil.*

⁹⁾ *Department of Mathematics and Statistics, State University of Ponta Grossa, 84030-900, Ponta Grossa, PR, Brazil.*

In this work, effects of constant and time-dependent vaccination rates on the Susceptible-Exposed-Infected-Recovered-Susceptible (SEIRS) seasonal model are studied. Computing the Lyapunov exponent, we show that typical complex structures, such as shrimps, emerge for given combinations of constant vaccination rate and another model parameter. In some specific cases, the constant vaccination does not act as a chaotic suppressor and chaotic bands can exist for high levels of vaccination (e.g., > 0.95). Moreover, we obtain linear and non-linear relationships between one control parameter and constant vaccination to establish a disease-free solution. We also verify that the total infected number does not change whether the dynamics is chaotic or periodic. The introduction of a time-dependent vaccine is made by the inclusion of a periodic function with a defined amplitude and frequency. For this case, we investigate the effects of different amplitudes and frequencies on chaotic attractors, yielding low, medium, and high seasonality degrees of contacts. Depending on the parameters of the time-dependent vaccination function, chaotic structures can be controlled and become periodic structures. For a given set of parameters, these structures are accessed mostly via crisis and in some cases via period-doubling. After that, we investigate how the time-dependent vaccine acts in bi-stable dynamics when chaotic and periodic attractors coexist. We identify that this kind of vaccination acts as a control by destroying almost all the periodic basins. We explain this by the fact that chaotic attractors exhibit more desirable characteristics for epidemics than periodic ones in a bi-stable state.

Mathematical models are a powerful tool to study the spread of diseases and strategies to control them. In the present contribution, we examine the effects of constant and time-dependent vaccination campaigns on the dynamical behaviour of a seasonal forced Susceptible-Exposed-Infected-Recovered-Susceptible (SEIRS) model. The impacts of such strategies are investigated through Lyapunov exponents for parameter planes. We discover that typical complex structures, emerge for constant vaccination and for a certain parametric configuration. The structures observed in the parameters planes show very complex dynamics in the model. Next, we use parameters for chaotic and bi-stable solutions and explore the influence of a time-dependent immu-

nisation program. We uncover that the time-dependent vaccination campaign can control the chaotic bands, making them periodic under specific conditions. Using a parametric configuration that generates bi-stable solutions where periodic-periodic and chaotic-periodic attractors coexist, we investigate the effects of a time-dependent immunisation campaign on the dynamics. For this, we develop a method to select one attractor over another. Additionally, our results show that chaotic attractors spend more time at low infection levels than periodic ones for the same parametric configuration.

^{a)} Electronic mail: ecgabrick@gmail.com

I. INTRODUCTION

Vaccination is one of the most efficient ways to control disease spreading¹. For example, in United Kingdom (UK) the reported annual cases of measles in the pre-vaccination were around 100,000 to 800,000, but after the introduction of vaccination in 1968 the reported cases decreased to 30,000 per year, from 1968 up to 1988². More recently, it was estimated that COVID-19 vaccination prevented around 14 million deaths in 185 countries, from Dec. 2020 to Dec. 2021³.

Vaccine campaigns can be conducted by different strategies. One is the mass vaccination campaign which consists of vaccinating a large number of people in a short time⁴. Another is to vaccinate different groups in discrete time intervals, namely pulsed vaccination⁵. Moreover, some diseases are seasonal and are better controlled by combining seasonal vaccination with routine campaigns⁶, i.e., make them time-dependent. Such strategies have been shown useful against certain diseases⁷, especially seasonal ones⁸. When they are combined with routine programs, the time-dependent term causes perturbations that can drive the system to a new equilibrium situation⁹.

One form to decide the vaccination strategy is by means of mathematical models¹⁰, once these tools are powerful for modelling and studying mitigation strategies for epidemic spread¹¹. In this way, mathematical models bring very important insights for the elaboration of campaigns. In a situation where two vaccine doses need to be administrated, the models suggest that is better to discriminate the population before applying the vaccine¹². With this procedure, a smaller amount of doses is needed to reach the same effects as when they are applied randomly. In addition, if the vaccine is applied in a pulsed protocol, the number of wasted doses is drastically reduced. When seasonal effects are taken into account in the contact rates, pulsed vaccine combined with routine is more efficient than just routine vaccine¹³. Many works have been done in terms of vaccination strategies^{14–19}. However, there are only few works dedicated to understand the dynamical behaviour of such systems.

Under constant vaccination protocols, the SIR model with logistic growth can produce complex dynamics for a set of parameters²⁰. These solutions exhibit different kinds of bifurcation such as Hopf, transcritical, Belyakov and saddle-node, depending on the basic reproduction number (R_0) and the proportion of vaccinated individuals. When pulses are incorporated into the vaccination strategy, solutions of disease-free (DFE) can be obtained depending on the rates²¹. Moreover, the system is driven to chaotic solutions in the presence of seasonal variations. The chaotic solutions generated due to the seasonal forcing can be controlled to periodic motion when a seasonal component is added to the vaccination strategy²². For a general periodic vaccination rate, periodic DFE solutions are ensured when $R_0 < 1$ and have the same period as the vaccine function²³. DFE solutions are globally asymptotically stable for $R_0 < 1$ in a situation where

the period of vaccination function is a multiple integer of the seasonal contact rate. Nonetheless, this solution becomes unstable for $R_0 > 1$ ²⁴. In a SEIRS seasonal model, chaotic and bi-stable solutions can emerge for constant and pulsed vaccination rates²⁵.

In this work, we study the dynamical behaviour of a seasonal forced SEIRS model under constant and non-constant (seasonal) vaccination rates. We explore the dynamical properties in a wide range of parameters and present a control method for bi-stability. In this way, this research is a strong generalization of a previous paper about the effect of the constant and pulsed protocol of vaccination rates²⁵. We investigate the effects of constant and time-dependent vaccination rate into the dynamical behaviour of a seasonal SEIRS model, aiming to understand the following questions: (i) Could the constant vaccination rate suppress chaotic dynamics? (ii) What are the effects of vaccination types in the bi-stable range?

To explore these questions, we split this work into two parts. In the first one, for a constant vaccination protocol, we verify that chaotic solutions can be produced even for high vaccination rates depending on the other parameters. Furthermore, we show that under specific conditions some typical complex structures such as shrimps²⁶ emerge. This typical complex structures were firstly named by J. A. C. Gallas²⁶. In terms of bi-stability, we find that the seasonal vaccination can act as a control method. This control enables us to select the attractors as a function of the vaccination parameters. In addition, periodic basins can be destroyed due to high levels of infection.

We organise this work as following: In Section II, we present the model and discuss some aspects of its equilibrium. Section III is dedicated to show the results related to constant vaccination. The seasonal vaccination rate is described in Section IV and its influence on bi-stable solutions is discussed in Section V. Finally, we draw our conclusions in Section VI.

II. MODEL

Given a population of size N , the SEIRS model splits the population according to their infectious status, which are Susceptible (S), Exposed (E), Infected (I), and Recovered (R)²⁷. Healthy individuals are stored in S , infected but not infectious in E , infectious in I , and recovered in R ¹. Originally, this model did not include vaccination²⁸. However, this can be done by transferring newborns and other S individuals to R compartment²⁹, as schematically represented in Fig. 1. The arrows indicate the flow between the compartments, where the parameters are: b birth rate; β contact rate of between S and I individuals; $1/\alpha$ latent period; γ recovery rate; $1/\delta$ time to loss the immunity; μ natural death rate; κ vaccine efficacy; p newborns vaccination rate; and v_0 rate at which S individuals are vaccinated. Without loss of

generality, we use $\kappa = 1$ in this whole work. Observe that the fraction bpN that is introduced in R came from the vaccination in the S newborns.

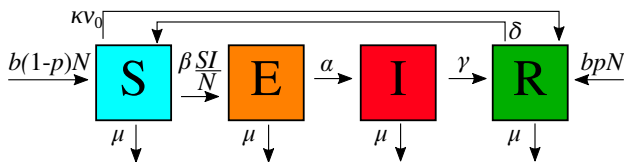


FIG. 1. Representation of SEIRS model with vaccination.

The representation in Fig. 1 shows the compartments S , E , I , and R in capital letters, which represent the number of individuals in each compartment, from a given population N . From the modelling point of view, we can work with the model independent of N . To do that, we write the equations in terms of the fractions s , e , i , and r . A complete discussion about the normalization is given in Ref.³⁰. The normalised SEIRS is described by the following system of ordinary differential equations

$$\frac{ds}{dt} = b(1-p) - \beta si + \delta(1-s-e-i) - \mu s - \kappa v_0 s, \quad (1)$$

$$\frac{de}{dt} = \beta si - (\alpha + \mu)e, \quad (2)$$

$$\frac{di}{dt} = \alpha e - (\gamma + \mu)i, \quad (3)$$

where we assume $b = \mu$, then, $r = 1 - s - e - i$. For more details about the equilibrium solutions and properties of Eqs. (1)-(3) refer to¹³.

We consider a time-dependent contact rate given by

$$\beta \equiv \beta(t) = \beta_0 [1 + \beta_1 \cos(\omega t)], \quad (4)$$

where β_0 is the average contagion rate, $\beta_1 \in [0, 1]$ is the seasonality degree, and ω is the frequency. This formulation is taken to model seasonal infectious diseases transmission³¹⁻³³.

The main novelty of this work is to explore effects of a seasonal vaccination, that is modelled by the continuous function:

$$v(t) = v_0 + \xi \cos(\omega_v t), \quad (5)$$

where $\xi \in [0, v_0]$ is the amplitude and ω_v is the frequency of the vaccination campaign. Observe that when $\xi \ll 1$ the vaccination campaign is predominantly given by v_0 but with a periodic perturbation. The period of vaccination is given by $T_v = 2\pi/\omega_v$ in years unity.

The complete model is described by Eqs. (1)-(3) together to Eq. (4) and (5). For biological reasons, the initial conditions and the parameters present in Eqs. (1)-(3), (4) and (5) are ≥ 0 . Then, the solutions are bounded in the set: $D = \{(s, e, i) \in [0, 1]^3\}$ for every $t \geq 0$ (Ref.³⁴). The solutions are numerically obtained by 4th order Runge-Kutta method³⁵ with the integration step equal to 10^{-3} .

Figure 2 displays numerical solutions for $b = 0.02$, $p = 0.25$, $\kappa = 1$, $v_0 = 0.2$, $\beta_0 = 800$, $\beta_1 = 0.20$, $\omega = 2\pi$, $\alpha = 40$, $\gamma = 100$, $\delta = 0.25$, and $\xi = 0$. The blue, black, red, and green lines show the respective solutions for s , e , i , and r variables. This result is for the interval of 10 years, discarding the first 10 years of transient. The solution is oscillatory with a period equal to 2π .

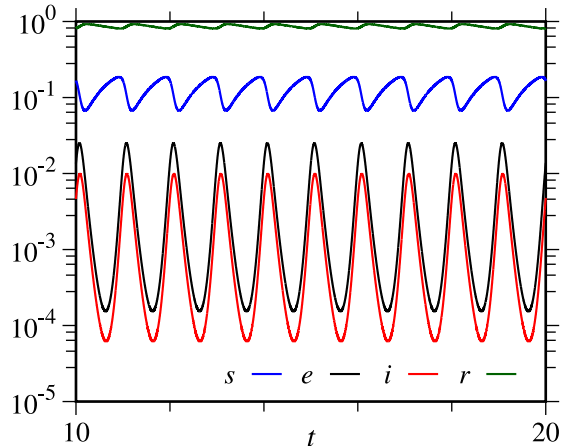


FIG. 2. Numerical solution for SEIRS model. The blue, black, red, and green lines are for s , e , i , and r , respectively. We consider $b = 0.02$, $p = 0.25$, $\kappa = 1$, $v_0 = 0.2$, $\beta_0 = 800$, $\beta_1 = 0.20$, $\omega = 2\pi$, $\alpha = 40$, $\gamma = 100$, $\delta = 0.25$, and $\xi = 0$.

III. DYNAMICAL BEHAVIOUR FOR $\xi = 0$

First, we study the effects of a constant vaccination rate on the dynamical system, i.e., $\xi = 0$ in Eq. (5).

The influence of v_0 on the dynamical system behaviour is measured by the associated Lyapunov exponents computed for each pair $v_0 \times [\cdot]$, where $[\cdot]$ is one parameter from the model. In this work, we display the Lyapunov exponents in colour scale. When the Lyapunov exponents are greater than zero, we plot the first largest one and when they are smaller than zero, we plot the second largest. We follow this procedure due to the fact that the transformation from non-autonomous to autonomous systems gives us a null exponent³⁰. We use the Wolf algorithm to compute the Lyapunov exponents³⁶ under initial conditions equal to $s_0 = 1 - e_0 - i_0$, $i_0 = 10^{-3}$, $e_0 = 0$. The Lyapunov exponents showed in this research are limited in the range $[-0.4 : 0.4]$ to obtain a standard colour code. Nonetheless, it is important mentioning that the exponents can be lower or higher than this range. The transient is fixed as 5×10^5 integration steps.

Figure 3 exhibits the results for the parameter planes $v_0 \times \alpha$ and $v_0 \times \gamma$, in the panels (a) and (b), respectively. The colour scale indicates the Lyapunov exponent (λ). DFE (disease-free) solutions are separated from non-DFE ones by the dotted magenta curve. To numerically verify the DFE, we compute the area under i and e curves.

When both are less than 10^{-6} , we obtain a DFE solution. Inspired by the minimal vaccination coverage obtained by Gabrick et al.¹³, we fit the numerical result for DFE using a function $v_0(\alpha) = a/(1+b\alpha^{-1})+c$, obtaining $a = 0.7089 \pm 0.0001$, $c = 0.2702 \pm 0.0001$, where b is the birth rate. Comparing with Eq. (13) from Ref.¹³, we get $v_0(\alpha) = 0.715/(1 + 0.02\alpha^{-1}) - 0.27$. These results show that α has an influence on DFE only for small values. For a fixed α , variations of v_0 can lead the system from a periodic dynamics to chaotic via period-doubling, such as the points marked by the gray squares. Additionally, v_0 can lead the system back to periodic behaviour via crisis³⁷ in some points, such as the points delimited by the green circles. For a certain range of parameters, we observe the coexistence between periodic and chaotic attractors. When we compute the total number of infected individuals in the periodic or chaotic regime in the same time window, our results show that this number is practically the same for these parameter configurations. These results lead us to conclude that the total number of infected individuals is independent whether the dynamics are chaotic or periodic.

Fixing $\alpha = 100$ and varying γ , we get the result shown in Fig. 3(b). The DFE separation is given by a non-linear expression equal to $v_0(\gamma) = a/(\gamma+b)+c$, with $a = 70.47 \pm 0.02$, $c = 0.2699 \pm 0.0002$, and b is the natural birth. This relation establishes $v_0 \propto \gamma^{-1}$ as a threshold for DFE. The power-law behaviour can be understood by the fact that as the measure γ increases faster the individuals go to R , which helps to obtain DFE once the other parameters are not able to sustain a endemic state. On the other hand, as γ decreases until $\gamma = 56.56$, more vaccination is needed to obtain DFE. For values $\gamma < 56.56$ even with $v_0 = 1.0$ there is no DFE. Contrary to the result in panel (a), the type of dynamics is more stronger dependent on the combination of v_0 and γ . Nonetheless, for a fixed γ value, period-doubling bifurcations and crisis also can be found, as marked by the gray squares and green circles, respectively. We also observe that the total number of infected does not change whether the dynamics is chaotic or periodic.

As previously observed, combinations of $v_0 \times \alpha$ lead to rich typical complex structures, such as shrimps, highlighted by the small cyan square in Fig. 3(a). A magnification of this structure is display in Fig. 4. Shrimps are periodic structures immersed into chaotic bands^{38,39}. As far we know, in epidemiological models the emergence of such structure was first reported in Ref.³⁰. Shrimps are important features because in their vicinity can happen cascades of similar periodic structures leading to a chaotic route⁴⁰. Close to shrimps, small changes in the parameters can drastically alter the dynamic⁴¹. In our case, the main body of the structure has period 5.

Figure 5 exhibits the results for the combinations $v_0 \times \beta_0$ (panel (a)) and $v_0 \times \delta$ (panel (b)) as a function of λ in the colour scale. These outcomes are for constant vaccination. For both panels, the DFE solution is delimited by a linear relationship given by $v_0(x) = ax + c$.

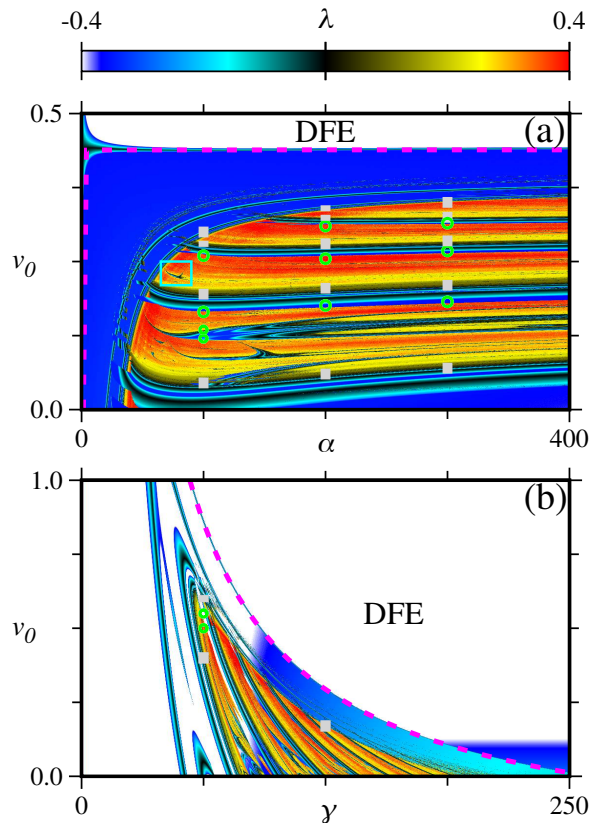


FIG. 3. Influences of constant vaccination rate (v_0) and α , in the panel (a) for $\gamma = 100$; and $v_0 \times \gamma$, in the panel (b) for $\alpha = 100$, in the Lyapunov exponent (λ), in colour scale. We consider $b = 0.02$, $\omega = 2\pi$, $\delta = 0.25$, $\beta_0 = 270$, $\beta_1 = 0.28$, and $p = 0.25$. Green circles and grey squares highlight transitions by crisis and period-doubling, respectively. The cyan square highlighted in the panel (a) is magnified in Fig. 4.

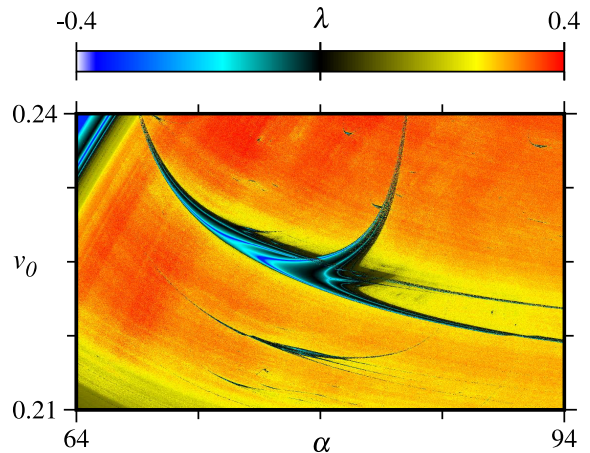


FIG. 4. Magnification of a shrimp highlighted by the cyan square in Fig. 3(a), for constant vaccination. We consider: $b = 0.02$, $\omega = 2\pi$, $\delta = 0.25$, $\beta_0 = 270$, $\beta_1 = 0.28$, $\gamma = 100$, and $p = 0.25$.

When $x = \beta_0$, we obtain $a = 0.002 \pm 9 \times 10^{-7}$, $c =$

-0.2701 ± 0.0003 , and for $x = \delta$: $a = 1.6724 \pm 0.0004$ and $c = 0.1848 \pm 0.0001$. The parameters are very close to the ones yielded directly from the theoretical result (Eq. (13) in Ref.¹³). The apparent similarity of the results generated by varying β_0 and δ also occurs in the absence of vaccination^{25,30}. As in the previous results, some bifurcations via period-doubling and crisis also are highlighted by grey squares and green circles. For $\beta_0 \geq 488.5$ only non-DFE solutions occur even for $v_0 > 0.95$ (Fig. 5(a)). Additionally, chaos is observed for $v_0 > 0.95$ in the range $\beta_0 \in (560, 614)$. This result shows that v_0 does not act as controlling chaos. For $\beta_0 > 604$ only periodic solutions remain, independent of v_0 . In this case, a high contact rate leads to periodic solutions. Fixing $\beta_0 = 270$ and varying δ , only periodic solutions exist for $\delta > 0.624$ (Fig. 5(b)). Therefore, when the lost of immunity occurs for periods less than 1.6 years, the dynamic is periodic. On the other hand, diseases with a lost of immunity greater than 1.6 can generate chaotic dynamics.

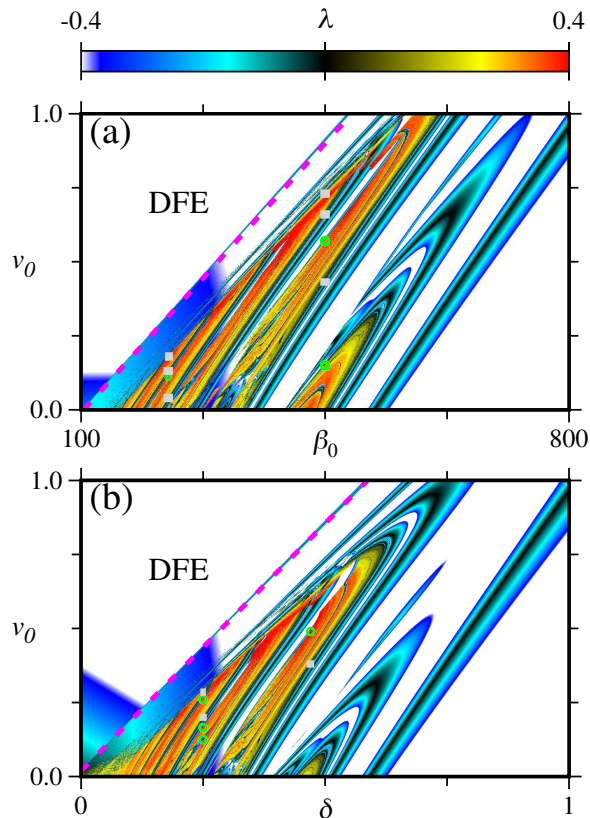


FIG. 5. Influence of constant vaccination rate (v_0) and β_0 , in the panel (a) for $\delta = 0.25$; and $v_0 \times \delta$, in the panel (b) for $\beta_0 = 270$, in the Lyapunov exponent (λ), in colour scale. We consider $b = 0.02$, $\omega = 2\pi$, $\gamma = 100$, $\alpha = 100$, $\beta_1 = 0.28$, and $p = 0.25$. Green circles and grey squares highlight crisis and period-doubling bifurcations, respectively.

Another constant relationship that separates DFE solutions from endemics ones is obtained by varying ω (Fig. 6(a)). In this case, the threshold is independent of ω and is given by $v_0 = 0.44$. For $v_0 < 0.44$ and $\omega \in (0.48, 3.26)\pi$

the solutions can be periodic or chaotic. Outside this range, there are only periodic solutions. For a given ω in the chaotic band, the increase of v_0 can suppress the chaotic behaviour. After some transient, the total infected only depends on v_0 . One important value of this parameter is 2π . We observe some transitions in the dynamics induced by crisis (green circles) and period-doubling (grey square).

As our last analyses of the parameter plane, we fix $\omega = 2\pi$ and vary β_1 , as shown in Fig. 6(b). For this result, the DFE is not described by the relation obtained in Ref.¹³. This is expected once this minimum coverage is derived for non-autonomous model. Here, we give a contribution showing that for $\beta_1 > 0.5$ a non-linear contribution appear. Now the separation from DFE to endemic can be described by $v_0(\beta_1) = a + c\beta_1 + d\beta_1^e$, with the parameters $a = 0.4398 \pm 0.0003$, $c = 0.7103 \pm 0.0006$, $d = -0.8114 \pm 0.0006$, and $e = 1.108 \pm 0.001$. In this sense, an analytical expression for the minimum coverage for the forced model remains an open question. The non-linear contribution appears because for high levels of β_1 combined with v_0 the DFE is reach earlier. Chaotic solutions are found only for $v_0 < 0.38$ and $\beta_1 > 0.12$. Additionally, chaotic orbits depends are strongly dependent of β_1 . Fixing $\beta_1 = 0.5$ and varying v_0 , we observe many chaotic bands, that emerge from crisis or period-doubling bifurcation and are marked by green circles and grey squares, respectively.

IV. SEASONAL VACCINATION

Now, we consider the effects of a time-dependent vaccination campaign, i.e., ξ and $\omega_v \neq 0$ in Eq. (5). However, to obtain the chaotic and bi-stable solutions we construct a bifurcation diagram for a constant vaccination rate by recording i in the stroboscopic section as a function of β_1 .

Figure 7 displays the bifurcation diagram for β_1 and a constant vaccination rate $v_0 = 0.1$. The y -axis shows the i variable in the stroboscopic section. We select these parametric configuration because the richness of the dynamical behaviour. The red and blue points are recorded in the forward and backward directions of β_1 , showing a hysteresis curve⁴². The grey background highlighted the bi-stable regions, which will be investigated in Section V. In the absence of vaccination, for $\beta_1 > 0.9$ only chaotic solution is obtained^{25,30}. For the considered parametric configuration and for $v_0 = 0.1$ a periodic solution emerges for high levels of β_1 . It is worth mentioning that for other values of v_0 chaotic orbits can be found in this range (Fig. 6(b)). To explore the effects of ξ and $\omega_v \neq 0$ in the chaotic bands, we consider three levels of seasonality degree, which we define by: high $\beta_1 \in [0.7, 1]$, medium $\beta_1 \in (0.3, 0.7)$ and low $\beta_1 \in [0, 0.3]$. In the next subsection we discuss in the following all of them.

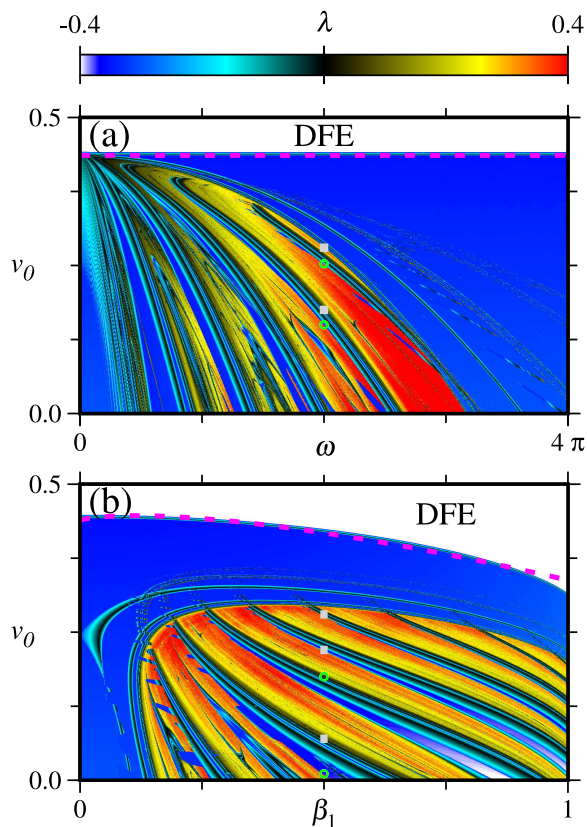


FIG. 6. Effects of constant vaccination rate (v_0) and ω , in the Lyapunov exponent (λ), in colour scale. We consider $b = 0.02$, $\delta = 0.25$, $\gamma = 100$, $\alpha = 100$, $\beta_0 = 270$, and $p = 0.25$. Green circles and grey squares highlight transitions by crisis and period-doubling, respectively.

A. Low seasonality degree

Considering a seasonal vaccination campaign (Eq. (5) with ξ and $\omega_v \neq 0$), we investigate how the chaotic solution for low seasonality ($\beta_1 = 0.15$) is affected. Figure 8(a) displays the parameter plane $\xi \times \omega_v$ as a function of λ in colour scale. It is important to note that in Fig. 8(a), as well as in Fig. 9(a) and Fig. 10, the top x -axis exhibits the period T_v in months, where we mark the points in which periodic bands emerge. In Fig. 8(a), we observe the existence of four periodic bands, namely I, II, III, and IV. These bands occur for, and near, $\omega_v (T_v) = 2.094$ (36.00), 2.512 (30.01), 3.139 (24.02) and 3.771 (20.00). We select these points to analyse because they represent a richer dynamics than their neighbours. It is important to note that some periodic bands are narrower than others. The first two bands, I and II, are magnified in the panel (a).

Fixing $T_v = 36.00$, we increase ξ from 0.02 up to 0.10, then a crisis is found at $\xi \approx 0.076$, which is marked by the green circle in Fig. 8(a). At this point, the chaotic attractors coalesce in a periodic branch with period 1. For which the amplitude of the i variable in stroboscopic

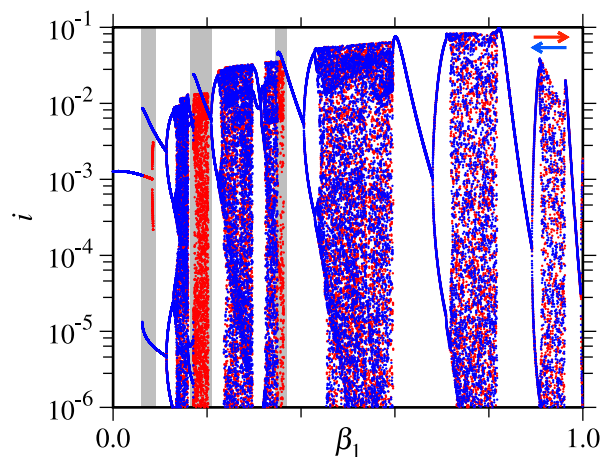


FIG. 7. Bifurcation diagram type hysterereses for β_1 considering a constant vaccination rate $v_0 = 0.1$. The points are recording in the stroboscopic section. The red points are in the forward and the blue in the backward direction of β_1 . The gray background delimits the bi-stable solutions. We consider $b = \mu = 0.02$, $\alpha = 100$, $\gamma = 100$, $\omega = 2\pi$, $\delta = 0.25$, $\beta_0 = 270$, and $p = 0.25$.

section decreases until 0.0056 in $\xi = 0.1$.

Following ω_v in the positive direction, we reach the periodic band II (Fig. 8(a)). It displays more complex dynamics when compared with I. For $T_v = 30.01$ and increasing ξ in the range from 0.02 to 0.1, a crisis occurs at $\xi \approx 0.027$, and the chaotic attractor becomes periodic with period 1. The attractor with period 1 doubles the period at $\xi \approx 0.042$, which is denoted by a horizontal white line in panel (a). The period 2 attractor suffers another period-doubling bifurcation at $\xi \approx 0.055$. The 4-period attractor ends in $\xi \approx 0.06$ and many subsequent period-doubling bifurcations occur, which we denote by the three white dots in the panel (b). For this value of T_v , the chaotic attractor becomes periodic via a crisis (increasing ξ) and then returns back to chaos via period-doubling bifurcation. The return to chaos occurs in the range $\xi \in (0.064, 0.1]$. The i amplitude in the stroboscopic section is higher in the chaotic regime than in the periodic one.

The bands III and IV are magnified in Fig. 8(c). To explore the dynamic associated with the band III, we consider $T_v = 24.02$ and vary ξ . The chaotic attractor disappears via a crisis at $\xi \approx 0.056$ giving rise to a 5-period attractor until $\xi \approx 0.067$. For $\xi > 0.067$ the period of the attractor changes to 3 and stays there for the whole analyzed range. We analyse the last band, namely IV, by considering $T_v = 20$. A crisis occurs at $\xi \approx 0.039$ and the chaotic attractor changes to a periodic one with period equal to 2. This period does not change in the considered range. The bands III and IV leave the system near to DFE. In $\xi = 0.1$, the period 3 branch for III oscillates among $i = 0.0016$, 0.000009, and 0.006842 in the stroboscopic section. For the same value of ξ and for IV the dynamic oscillates between $i = 0.006025$ and

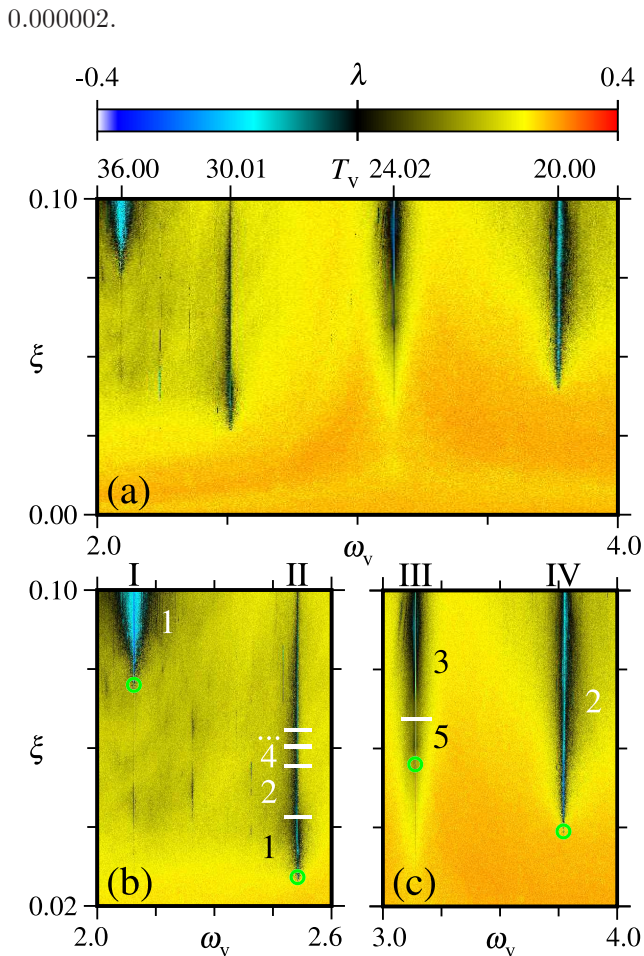


FIG. 8. Impacts of seasonal vaccination in chaotic attractor for $\beta_1 = 0.15$. Panel (a) display the parameter plane $\xi \times \omega_v$ where the colour scale indicates the Lyapunov exponents (λ). The panels (b) and (c) exhibit the magnification of periodic bands from the panel (a). We consider $b = 0.02$, $\alpha = 100$, $\gamma = 100$, $\omega = 2\pi$, $\delta = 0.25$, $\beta_0 = 270$, $p = 0.25$, and $v_0 = 0.1$.

B. Medium seasonality degree

To evaluate the seasonal vaccination campaign in a medium seasonality degree, we fix $\beta_1 = 0.5$. For this parameter, 7 periodic bands emerges in the range $\omega_v \in [0.25, 1.70]$ ($T_v \in [301.59, 43.084]$), as shown in Fig. 9(a). The bands I', II', and III' are magnified in the panel (b), while IV', V', VI', and VII' in the panel (c). Each band occupies a certain range in the ω_v (T_v) parameter. Nonetheless, we select some values to locate each periodic branch. Focusing in the panel (a) and fixing $\omega_v = 0.349$ ($T_v = 216.04$), if we increase ξ from 0 to 0.1 direction, we find a crisis point marked by the magenta circle that gives the origin for the band I'. The crisis occurs at $\xi \approx 0.07$ where the chaotic attractor coalesces in a periodic branch with period 1 and remains there until the analysed range ($\xi = 0.1$). This periodic

branch oscillates sinusoidal reaching a minimum value in the stroboscopic section equal to $i = 0.016$. Thereafter, it starts increasing again.

The periodic band II' can be obtained with $\omega_v = 0.609$ ($T_v = 123.80$) and varying ξ (Fig. 9(b)). In this case, the chaotic band goes to a 1-periodic attractor in $\xi \approx 0.058$ and remains there until $\xi = 0.07$. For values $\xi > 0.07$ this band returns to the chaotic attractor. In the stroboscopic section, the periodic branch oscillates sinusoidal in $\xi \in (0.058, 0.07)$, having the first minimum local point in the pair $(\xi, i) \approx (0.061, 0.008)$. After that, it increases until a maximum in $(\xi, i) \approx (0.065, 0.037)$. From $\xi > 0.065$ until $\xi = 0.07$, the stroboscopic section in i decays and remains practically constant for $i \approx 0.0003$.

To investigate the band III', we set $\omega_v = 0.698$ ($T_v = 108.02$) (Fig. 9(b)). It occurs a crisis at $\xi \approx 0.01$ where the chaotic attractor go to 1-periodic attractor until $\xi \approx 0.031$. At this point, it occurs a bubble bifurcation and the attractor starts to have period 2 until $\xi \approx 0.053$. After that, the attractor returns to period 1. The bifurcations are delimited in Fig. 9(b) by the white horizontal line.

Now, we analyse the range $\omega_v \in [1.05, 1.6]$ ($T_v \in [71.807, 47.123]$), which is displayed in Fig. 9(c). The bands IV', V', VI', and VII' are narrow in ω_v (T_v) when compared with I', II', and III'. Considering $\omega_v = 1.122$ ($T_v = 67.19$), we get the band IV', in which a 1-periodic attractor is created at $\xi \approx 0.085$ via a crisis. It is important to note that the 1-periodic attractor changes its amplitude for $\xi > 0.0894$, which is delimited by the horizontal white line. Moreover, the attractor does not changes suddenly the amplitude. First, it occurs a period-doubling bifurcation in $\xi = 0.0885$ and a new bifurcation in $\xi = 0.0887$ for a periodic attractor with period 3. Just after $\xi > 0.0894$ that the attractor returns to period 1 with a different amplitude. We do not mark these bifurcations in the figure because it occupies a very short range in ξ . Following the 1-periodic attractor in the stroboscopic section for i , its amplitude increases linearly in the range $\xi \in [0.0894, 0.1]$, from $i \in [0.023, 0.027]$.

A small periodic band, called V', also exists for $\omega_v = 1.254$ ($T_v = 60.12$). The chaotic attractor goes to a 1-periodic attractor in the range $\xi \in (0.09, 0.1]$. The structure VI' exhibits an interest dynamics for $\omega_v = 1.398$ ($T_v = 53.93$). The chaotic attractor goes to a periodic attractor via a bifurcation that starts in $\xi \approx 0.05$. In the range $\xi \in (0.05, 0.08)$, the periodic band has period 1 and, at $\xi \approx 0.084$, a bifurcation occurs where the periodic attractor goes to period 2 and remains there.

Finally, the last band, namely VII' (Fig. 9(c)), shows the transition from chaotic behaviour to periodic via a bifurcation at $\omega_v = 1.571$ ($T_v = 48$). Our results show that the chaotic attractors go to periodic ones via periodic doubling bifurcation. However, there is a periodic branch that occupies the range $\xi \in (0.06, 0.1]$, for $i = 0.0004$ in the stroboscopic section. The chaotic attractor becomes periodic with period 5 in $\xi \in (0.082, 0.083)$, where for $\xi \approx 0.083$ a new bifurcation occurs, that is marked in the

panel (c) by the white horizontal line, and the periodic band becomes a 3-period until $\xi \approx 0.091$. At this point, a new bifurcation occurs and the attractor has period 2. One branch for $i = 0.04$ and another for $i = 0.0004$.

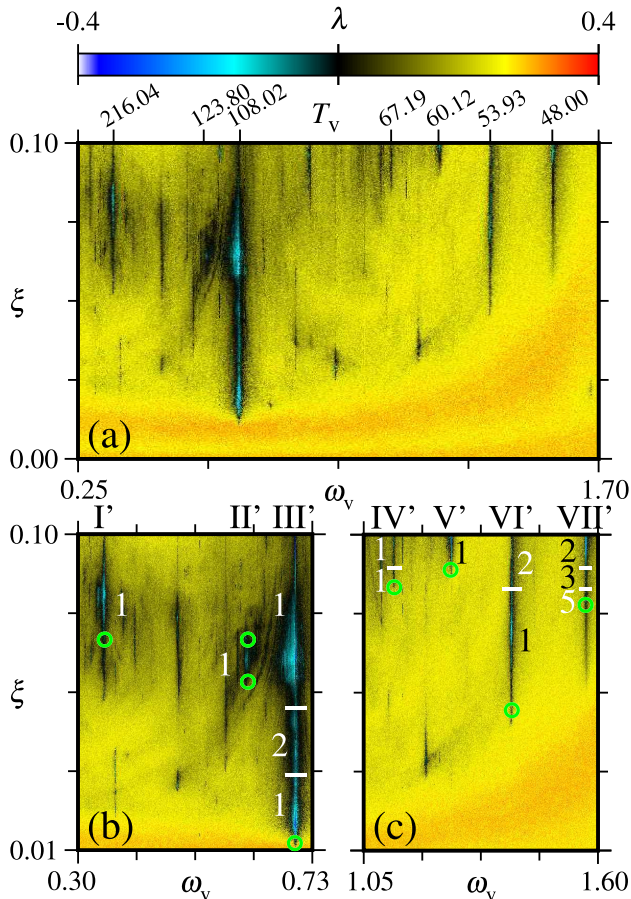


FIG. 9. Impact of seasonal immunisation program in the chaotic attractor for $\beta_1 = 0.5$. Panel (a) exhibit the parameter plane $\xi \times \omega_v$ as a function of Lyapunov exponent (λ), in colour scale. The periodic bands present in the panel (a) are magnified in panels (b) and (c). We consider $b = 0.02$, $\alpha = 100$, $\gamma = 100$, $\omega = 2\pi$, $\delta = 0.25$, $\beta_0 = 270$, $p = 0.25$, and $v_0 = 0.1$.

C. High seasonality degree

Considering a high seasonality degree in the contact function, e.g., $\beta_1 = 0.95$, it is possible to obtain two periodic bands in the range $\omega_v \in [0.8, 2]$ ($T_v \in [94.247, 37.699]$), denoted by I'' and II'' (Fig. 10). The band I'' is wider (in ω_v axis) and longer (in ξ axis) than II'' .

Fixing $\omega_v = 0.9$ ($T_v = 83.77$), we observe that the chaotic attractor changes to a 1-periodic attractor at $\xi \approx 0.02$ (Fig. 10). The periodic branch increases in its amplitude. For example, if we consider $\xi = 0.01$ (chaotic regime), the maximum amplitude of the attrac-

tor is 0.01, in the stroboscopic section for i . However, when the attractor changes the regime, the periodic attractor increases in amplitude reaching the maximum value $(\xi, i) = (0.025, 0.062)$. For $\xi > 0.025$, the i amplitude decreases until $i = 0.001$ in $\xi = 0.1$.

A different dynamics is generated by considering $\omega_v = 1.796$ ($T_v = 41.98$), which corresponds to a value inside the band II'' (Fig. 10). The chaotic attractor becomes periodic in $\xi \approx 0.07$, but the amplitude of the attractor decreases, in the i stroboscopic section from 0.07 (in chaotic regime) to 0.00004 (periodic behavior at $\xi = 0.071$). Increasing ξ , the amplitude of the periodic branch also increases and reaches the pair $(\xi, i) = (0.1, 0.095)$.

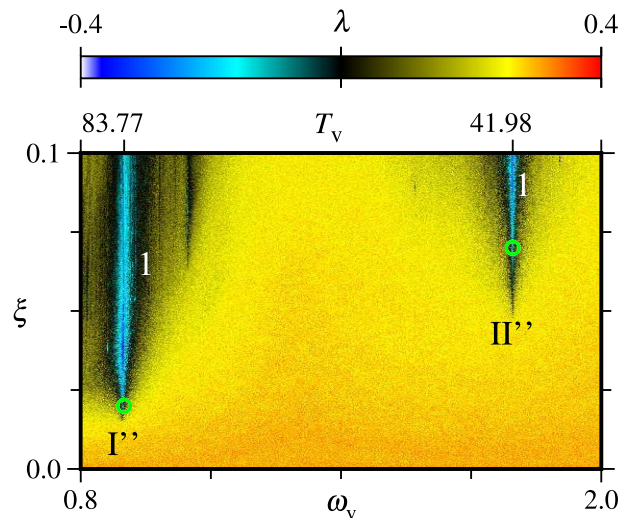


FIG. 10. Impact of seasonal immunisation campaign in the chaotic attractor for $\beta_1 = 0.95$. We consider $b = 0.02$, $\alpha = 100$, $\gamma = 100$, $\omega = 2\pi$, $\delta = 0.25$, $\beta_0 = 270$, $p = 0.25$, and $v_0 = 0.1$.

In Figs. 8, 9, and 10, some sparse points appear and the periodic bands are not well defined. By increasing the transient time or the number of iterations, we observe that the results remain unchanged. In this way, there is no transient effect present in the results.

V. INFLUENCE OF SEASONAL VACCINATION IN BI-STABILITY

In this section, we investigate the effects of a time-dependent immunisation program in the basin of a bi-stable solution. This is made by using ξ and $\omega_v \neq 0$ (Eq. 5) and the basins are computed in the bi-stable solution showed in Fig. 7.

Firstly, let us consider $\xi = \omega_v = 0$. From the result in Fig. 7, we observe three bi-stable regions, that are highlighted by the gray backgrounds. In our simulations, we consider $\xi = \omega_v = 0$ and $v_0 = 0.1$. These bi-stable regions shows the richness of the considered dynamical system⁴³. In this type of system the evolution is

extremely dependent on the initial conditions^{44,45}. For more details about bi and multi-stable system we refer to Refs.^{46–49}.

In Fig. 7, the first highlighted background shows the coexistence between two different periodic attractors in $\beta_1 \in (0.06, 0.09)$. After $\beta_1 \in (0.06, 0.083)$, it occurs a bifurcation to period 2 in the red attractor. We compute the basin of attractions considering the pair $e_0 \in [0, 1] \times i_0 \in [0, 1]$, and $s_0 = 1 - e_0 - i_0$, such that $s_0 + e_0 + i_0 \leq 1$. We discretized our space in a grid of 100×100 . The basin for $\beta_1 = 0.07$ is displayed in Fig. 11(a). Only in this basin we do not follow the colour code from Fig. 7. Instead, we mark the basin correspondent to the period 2 attractor by the orange colour and for period 1 by blue one. The white colour shows a prohibited region, where $s_0 + e_0 + i_0 + r_0 > 1$. Considering this mentioned discretization, we obtain 10000 possible initial conditions where 5050 evolve to one attractor or another. We call these 5050 initial conditions by valid points. We use the notation σ for the fraction that evolves to a period 1, Δ for the fraction that goes to period 2, and Γ for chaotic orbits. The period of the orbits is determined from the stroboscopic section. From the valid initial condition, a fraction equal to $\sigma = 0.23$ evolves to the attractor with period 1, while the remaining $\Delta = 0.77$ evolves to period 2 attractor.

The second bi-stable region is in $\beta_1 \in (0.17, 0.20)$ and exhibits the coexistence of a chaotic attractor, in the red branch, and a periodic one, in the blue branch. The basin for $\beta_1 = 0.18$ is displayed in Fig. 11(b). The red colour shows the pair (e_0, i_0) that evolves to a chaotic attractor, while the blue colour displays the pair that goes to a periodic regime. Considering the same procedure, the fractions are $\Gamma = 0.75$ and $\sigma = 0.25$. For $\xi = \omega_v = 0$, around 75% of the considered initial conditions evolve to the chaotic regime.

The last bi-stable range is in $\beta_1 \in (0.35, 0.365)$ where there is a coexistence between chaotic and periodic attractors. Figure 11(c) displays the basin of attraction for $\beta_1 = 0.36$. In this case, $\sigma = 0.26$ and $\Gamma = 0.74$, i.e., the chaotic attractor is preferable. Besides we have attractor with period 1 in each basin, is important observe that they are different.

Having the fraction of valid initial conditions that goes to period 1, 2, and chaos under constant immunisation campaign, we explore how these fractions change in relation to ξ and $\omega_v \neq 0$, i.e., a time-dependent campaign. To do this, we compute the basins by each pair $\xi \times \omega_v$ and the fraction σ . Then, we verify how σ depends on ξ and ω_v by looking at the parameter planes. We use the following colour code: $\sigma \in [0, 0.05]$ in black; $\sigma \in (0.05, 0.45]$ in yellow; $\sigma \in (0.45, 0.5]$ in white; $\sigma \in (0.5, 0.55]$ in cyan; $\sigma \in (0.55, 0.95]$ in blue; and $\sigma \in (0.95, 1]$ in purple. The intermediate colours shows the intermediates values.

Firstly, let us consider $\beta_1 = 0.07$, which corresponds to the basin in Fig. 11(a). Figure 12(a) displays the parameter plane $\omega_v \times \xi$ where the colour scale represents σ . For a long period, i.e., $T_v > 15.87$, it is possible to observe

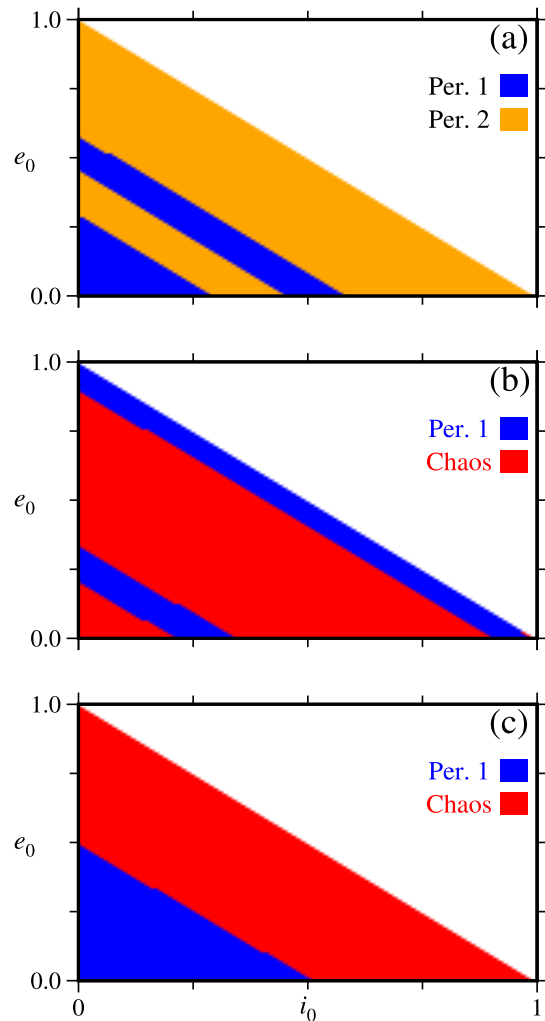


FIG. 11. Basin of attraction for constant vaccination campaign ($\xi = 0$). Each basin correspond to a section in Fig. 7, where the panel (a) is for $\beta_1 = 0.07$, (b) is for $\beta_1 = 0.18$, and (c) is for $\beta_1 = 0.36$. The blue colour shows points that evolve to periodic attractor with period 1, orange exhibit initial conditions that goes to period 2, and the red part is relative to chaotic attractors. We consider $b = 0.02$, $\alpha = 100$, $\gamma = 100$, $\omega = 2\pi$, $\delta = 0.25$, $\beta_0 = 270$, $p = 0.25$, and $v_0 = 0.1$.

a significant purple range, i.e., more than 95% of the valid points evolves to period 1 in this section. On the other hand, for $T_v < 7.93$, the initial conditions evolve, mostly, to the 2-period attractor. It is worth to mentioning that mostly part of this parameter plane is marked by orange colour, which means that approximately 20% of valid points goes to period 1.

Considering $\beta_1 = 0.18$, there is a bi-stable dynamics where chaotic and 1-period attractor coexist. Empliyng the same methodology that used to generate 11(a), we get Fig. 12(b). A significant part of the parameter plane is black, red, and orange. Meaning that $\sigma < 0.5$ for mostly combinations of ξ and ω_v . As previously observed, without seasonal terms in the vaccination rate, almost 75% of the 5050 initial conditions evolve to the

chaotic attractor. The preference by the chaotic attractor remains when we consider ξ and $\omega_v > 0$. Just small structures are in purple colour for $T_v > 15.87$.

Another bi-stable solution exist for $\beta_1 = 0.36$. A similar result is displayed in the panel (c). In this case, we do not observe purple tones, only cyan. The rest of the parameter plane contain orange, black, and red colours, meaning that $\sigma < 0.5$ for mostly part of $\xi \times \omega_v$.

The methodology employed and the results shows that seasonal vaccination works as a control of bi-stability⁵⁰⁻⁵².

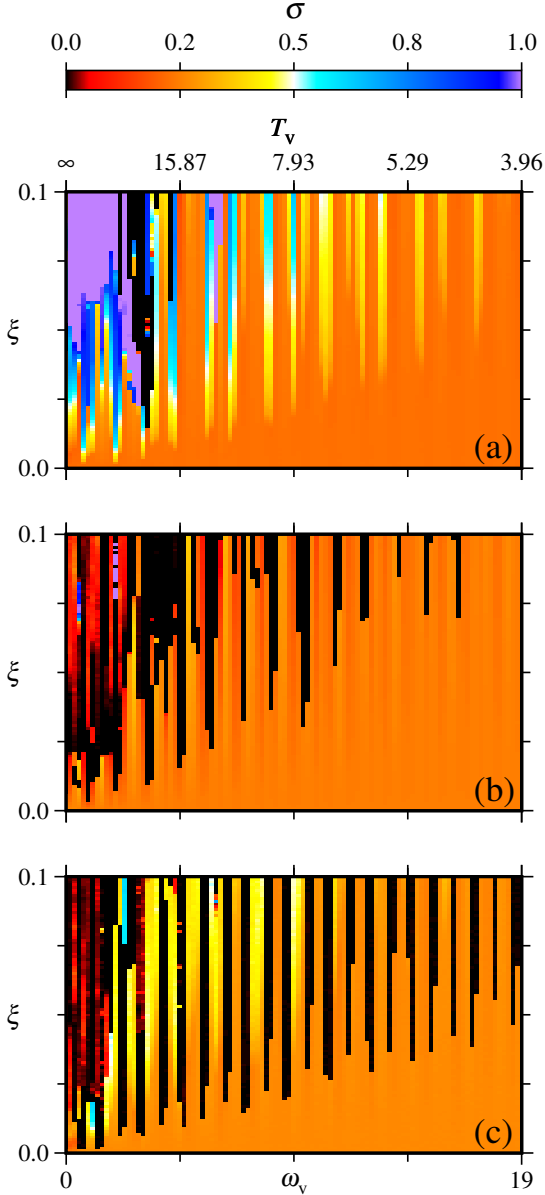


FIG. 12. Parameter plane $\xi \times \omega_v$. The colour scale displays the fraction of valid initial conditions that evolve to period 1 attractor (σ). The panel (a) is for $\beta_1 = 0.07$, (b) is for $\beta_1 = 0.18$, and (c) is for $\beta_1 = 0.36$. We consider $b = 0.02$, $\alpha = 100$, $\gamma = 100$, $\omega = 2\pi$, $\delta = 0.25$, $\beta_0 = 270$, $p = 0.25$, and $v_0 = 0.1$.

A. Why the chaotic attractors are preferred?

Our results in Figs. 12(b) and 12(c) shows that reaching the chaotic attractor is more preferable for the vaccination campaign. At this point, we need to understand the epidemics properties of periodic and chaotic attractors in an attempt to clarify why the chaotic attractors are preferred in this situations. As we observed in previous results, the total infected number is independent of chaotic or periodic attractors. However, for a given set of parameters, it is observed that chaotic attractors can have higher maxima values of infected individuals when compared with the periodic regime in the absence of vaccination³⁰. The same happen in presence of constant vaccination for some values of β_1 in the bi-stable range (Fig. 7). To understand which attractor is better in epidemic situations, we consider two bi-stable regions in $\beta_1 = 0.18$ (Bi-stability 2) and $\beta_1 = 0.36$ (Bi-stability 3), as displayed in Fig. 7.

One important characteristic in epidemic situations is the maximum point of infected individuals. In order to evaluate the local maximum points for the chaotic time series, we evolve the system during 2×10^5 iteration steps, discarding 10^6 as transient, over all the chaotic initial conditions according to Figs. 11(b) and (c). In total, we have 3803 and 3730 initial conditions for $\beta_1 = 0.18$ and $\beta_1 = 0.36$, respectively. Figure 13(a) shows the normalised frequency of maxima values of i for $\beta_1 = 0.18$. The red bar is related to chaotic time series while the blue is periodic. We normalise according to the higher frequency value. From this result, we observe that the maxima point for periodic orbit is always in 0.025 , while the chaotic are distributed in the interval $(10^{-6}, 0.017)$. The higher occurrence of maxima values of i for the chaotic attractor occurs for $i_{\max} < 10^{-5}$. Figure 13(b) displays a similar result for $\beta_1 = 0.36$. The values of i_{\max} for the chaotic initial conditions are distributed in the interval $(10^{-6}, 0.041)$, with higher occurrence for $i_{\max} < 10^{-5}$. By computing i_{\max} for the periodic initial conditions, we obtain a period 2, showing that the epidemic, in this case, is biannual, when we consider the section by the maxima points. In this case, we find $i_{\max} = 0.0484$ or $i_{\max} = 2 \times 10^{-6}$. From both of these results, we observe that chaotic attractors have less maximum value than periodic ones.

Another important measure is to know how long the attractor stays within limits of fewer and higher infections. As our model has the E compartment, it is important to evaluate i and e . Considering the same transient and the same initial conditions as in the previous case, we project the attractors in the plane $e \times i$ and establish thresholds in relation to i and e maxima values in the projection. We select the thresholds equal to 50% and 75% of these pairs. By means of the thresholds, we compute how long the time series stays below (t_B) and above (t_A) it. For the periodic case, the values are the same for every initial condition. For the chaotic situation, we see differences among the initial conditions, considering

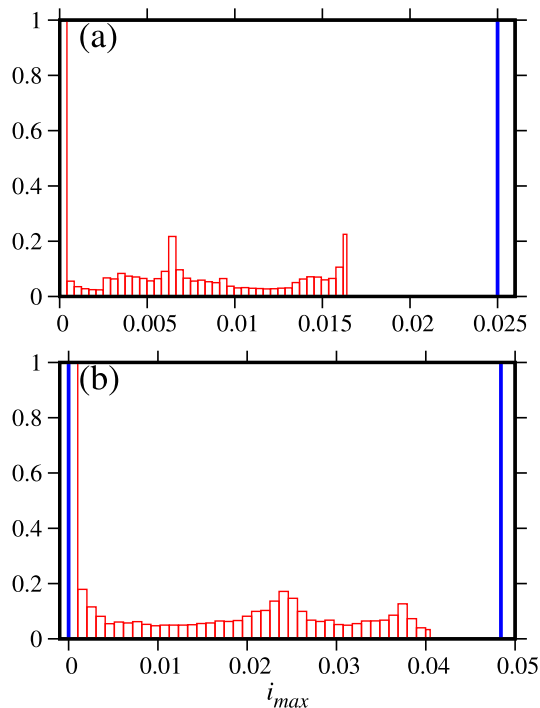


FIG. 13. Distributions of maxima i values for chaotic orbits (red bars) and periodic (blue bars) under constant vaccination ($v_0 = 0.1$). The panel (a) is for $\beta_1 = 0.18$ and the panel (b) for $\beta_1 = 0.36$. We consider $b = 0.02$, $\alpha = 100$, $\gamma = 100$, $\omega = 2\pi$, $\delta = 0.25$, $\beta_0 = 270$, $p = 0.25$, and $v_0 = 0.1$.

3803 different initial conditions for $\beta_1 = 0.18$ (chaotic part of Fig. 11(b)) and 3730 for $\beta_1 = 0.36$ (chaotic part of Fig. 11(c)). Table I displays the results for t_B and t_A for the periodic and chaotic attractor, for $\beta_1 = 0.18$ and $\beta_1 = 0.36$, respectively. The times are calculated for a window time equal to 200 years. Nonetheless, we verify that $t_B + t_A < 200$. The relation $t_B + t_A = 200$ does not occur because we are considering projections of the attractor. For both β_1 values, we observe that the chaotic attractor always spends more time below the threshold. For 50% and 75% the chaotic attractor also spends less time in the upper part of the attractor projection in $e \times i$. Combined with the information from Fig. 13, we show that, under specific conditions, the chaotic attractor can present low levels of infection compared with periodic orbits in some situations. Another important aspect when we are dealing with chaotic orbits is to know the horizon of predictability, which is $\propto 1/\lambda_1$. For $\beta_1 = 0.18$ and $\beta_1 = 0.36$, our simulations suggest 3.51 ± 0.15 and 3.02 ± 0.13 , respectively. Our results indicate that proportionally to 3 years, we can predict our time series, after that, we need more simulations. In terms of epidemic prediction, this is a very reasonable forecast horizon.

TABLE I. Time in which the periodic and chaotic attractor stay below (t_B) and above (t_A) the thresholds 50% and 75% set from the projection of the attractor in the plane (i, e) . For each chaotic attractor, we display the result $1/\lambda_1$ computed from 3803 and 3730 chaotic initial conditions, for $\beta_1 = 0.18$ and $\beta_1 = 0.36$, respectively. These results are for constant vaccination ($v_0 = 0.1$).

		$\beta_1 = 0.18$				
		Periodic		Chaos		
		t_B	t_A	t_B	t_A	$1/\lambda_1$
50%		72.89	7.90	147.28 ± 1.99	6.55 ± 0.28	3.51 ± 0.15
75%		76.11	4.69	151.78 ± 2.20	2.43 ± 0.15	–
		$\beta_1 = 0.36$				
		Periodic		Chaos		
		t_B	t_A	t_B	t_A	$1/\lambda_1$
50%		47.10	3.75	72.90 ± 2.67	2.61 ± 0.13	3.02 ± 0.13
75%		48.75	2.10	75.54 ± 2.62	0.51 ± 0.08	–

VI. CONCLUSIONS

In this work, we study a SEIRS model with a periodic time-dependent transmission rate. In the first part of the manuscript, we consider a constant vaccination rate in the model. The vaccination is applied into the susceptible individuals at a rate v_0 and in the newborns at p . Then, we compute the Lyapunov exponents for the combinations of v_0 and another parameter from the model. We verify relationships between v_0 and another parameters of the model that lead the system to disease-free (DFE) solutions. In terms of dynamical behaviour, we show that the parameter planes exhibit a very rich dynamics, showing chaotic and periodic structures, in particular shrimps. We discover that even for high values of v_0 (> 0.95), chaotic orbits exist.

Besides the mentioned contributions, the main novelty of the paper was given by extending the vaccination program by including a time-dependent function. With this modification, we obtain very important results. Firstly, we discover that parameters related to the time-dependent vaccination can drive the chaotic attractors to a periodic one by generating periodic structures in the parameter plane. In mostly cases, these structures are accessed via a crisis or period-doubling bifurcation.

It is important to mention that we use the stroboscopic section to build the bifurcation diagrams and obtain the bi-stable solutions. Nonetheless, it is also possible to use the maxima infected number as a section. In this case, the bi-stability appears in the same range of the bifurcation diagram and some periodic attractors can have different periods. Furthermore, recording the maxima infected number as a function of the control parameter, the periodic attractor mostly has a higher amplitude in the infected individuals when compared to chaotic attractors in the bi-stable windows.

By considering bi-stable solutions, between periodic-periodic and periodic-chaotic attractors, we propose a method to control these solutions based on the param-

eters of time-dependent immunisation program. This means that, with this methodology we can select one or other attractor as a function of vaccination parameters. We demonstrate that when chaotic and periodic attractors coexist, the basin of the periodic attractor is practically destroyed front a time-dependent immunisation campaign. This leads us to a new result. Despite chaos seems a bad feature in epidemiological models due to the unpredictability, we observe the opposite. For a considerable number of initial conditions, we show that in certain sections of the bi-stable dynamics, the maximum point of infected individuals is lower for the chaotic attractor. In addition, given a threshold in the attractor projection in the plane $e \times i$, we find that chaotic attractor spend more time in the inferior part and less time in the superior part of projection than period orbits. Furthermore, typically, the inverse of the largest Lyapunov exponent is proportional to 3 years.

The model discussed in this work shows very complex dynamics. One very characteristic important is the existence of a chaotic set in the multi-stable solution as an attractor and not as transient. Typically, in multi-stable systems chaotic attractors are difficult to be detected⁵³. In certain cases, the chaotic dynamics appear as long transients. In our system, transient chaos also is possible for a given parameter configuration. It is important to note that as our model is an epidemiological model, long simulation times can be considered more than 100 years. For the bi-stable solutions discussed in this work, we consider transients until 1000 years and the chaotic attractor remains unchanged. A similar result was observed in the same model without vaccination²⁵. The inclusion of a new forcing increases the nonlinearity of the system, as a consequence we observe an increase in the chaotic basin.

This works also adress some new problems. As far as we know, this is the second work that report the emergence of shrimps in epidemiological models (the first we refer to Ref.³⁰). In this way, questions like if this structure appear in other models or for some specific diseases remain open. Additionally, the structures reported in Fig. 12 need to be investigate more deeply.

ACKNOWLEDGEMENTS

The authors thank the financial support from the Brazilian Federal Agencies (CNPq); São Paulo Research Foundation (FAPESP) under Grant Nos. 2018/03211-6, 2020/04624-2, 2021/12232-0, 2022/13761-9, 2023/12863-5. Coordenação de Aperfeiçoamento de Pessoal de Nível Superior (CAPES); Fundação Araucária. E.C.G. received partial financial support from Coordenação de Aperfeiçoamento de Pessoal de Nível Superior - Brasil (CAPES) - Finance Code 88881.846051/2023-01. We thank 105 Group Science (www.105groupscience.com).

DATA AVAILABILITY

The data that support the findings of this study are available from the corresponding author upon reasonable request.

REFERENCES

- ¹M. J. Keeling and P. Rohani, *Modeling Infectious Diseases in Humans and Animals*, 1st ed. (Princeton University Press, Princeton, 2008).
- ²H. Jick and K. W. Hagberg, “Measles in the united kingdom 1990–2008 and the effectiveness of measles vaccines,” *Vaccine* **28**, 4588–4592 (2010).
- ³O. J. Watson, G. Barnsley, J. Toor, A. B. Hogan, P. Winskill, and A. C. Ghani, “Global impact of the first year of covid-19 vaccination: a mathematical modelling study,” *The Lancet Infectious Diseases* **22**, 1293–1302 (2022).
- ⁴J. D. Grabenstein and R. L. Nevin, “Mass immunization programs: Principles and standards,” in *Mass Vaccination: Global Aspects — Progress and Obstacles* (Springer Berlin Heidelberg, Berlin, Heidelberg, 2006) Chap. 3, pp. 31–51.
- ⁵Z. Agur, L. Cojocar, G. Mazor, R. M. Anderson, and Y. L. Danon, “Pulse mass measles vaccination across age cohorts,” *Proceedings of the National Academy of Sciences of the United States of America* **90**, 11698–11702 (1993).
- ⁶A. M. Roperó-Álvarez, H. J. Kurtis, M. C. Danovaro-Holliday, C. Ruiz-Matus, and J. K. Andrus, “Expansion of seasonal influenza vaccination in the americas,” *BMC Public Health* **9** (2009).
- ⁷P. J. Williams and H. F. Hull, “Status of measles in the gambia, 1981,” *Reviews of Infectious Diseases* **5**, 391–394 (1983).
- ⁸B. Greenwood, A. Dicko, I. Sagara, I. Zongo, H. Tinto, M. Cairns, I. Kuepfer, P. Milligan, J. B. Ouedraogo, O. Doumbo, and D. Chandramohan, “Seasonal vaccination against malaria: a potential use for an imperfect malaria vaccine,” *Malaria Journal* **16** (2017).
- ⁹F. A. B. Coutinho, E. Massad, M. N. Burattini, H. M. Yang, and R. S. A. Neto, “Effects of vaccination programmes on transmission rates of infections and related threshold conditions for control,” *Mathematical Medicine and Biology: A Journal of the IMA* **10**, 187–206 (1993).
- ¹⁰E. Massad, R. S. Azevedo-Neto, M. N. Burattini, D. M. T. Zanetta, F. A. B. Coutinho, H. M. Yang, J. C. Moraes, C. S. Pannuti, V. A. U. F. Souza, A. S. B. Silveira, C. J. Struchiner, G. W. Oselka, M. C. C. Camargo, T. M. Omoto, and S. D. Passos, “Assessing the efficacy of a mixed vaccination strategy against rubella in são paulo, brazil,” *International Journal of Epidemiology* **24**, 842–850 (1995).
- ¹¹R. M. Anderson and R. M. May, *Infectious diseases of humans: Dynamics and control* (Oxford University Press, Oxford, 1991).
- ¹²E. C. Gabrick, P. R. Protachevitz, A. M. Batista, K. C. Iarosz, S. L. T. de Souza, A. C. L. Almeida, J. D. S. Jr., M. Mugnaine, and I. L. Caldas, “Effect of two vaccine doses in the seir epidemic model using a stochastic cellular automaton,” *Physica A* **597**, 127258 (2022).
- ¹³E. C. Gabrick, E. L. Brugnago, S. L. T. de Souza, K. C. Iarosz, J. D. S. Jr., R. L. Viana, I. L. Cadas, A. M. Batista, and J. Kurths, “Impact of periodic vaccination in seirs seasonal model,” *Chaos* **34**, 013137 (2024).
- ¹⁴X. Liu, Y. Takeuchi, and S. Iwami, “Svir epidemic models with vaccination strategies,” *Journal of Theoretical Biology* **253**, 1–11 (2008).
- ¹⁵X. Wang, H. Peng, B. Shi, D. Jiang, S. Zhang, and B. Chen, “Optimal vaccination strategy of a constrained time-varying seir

- epidemic model,” *Communications in Nonlinear Science and Numerical Simulation* **67**, 37–48 (2019).
- ¹⁶C. J. E. Metcalf, J. Lessler, P. Klepac, F. Cutts, and B. T. Grenfell, “Impact of birth rate, seasonality and transmission rate on minimum levels of coverage needed for rubella vaccination,” *Epidemiol. Infect.* **140**, 2290–2301 (2012).
- ¹⁷M. Thäter, K. Chudej, and H. J. Pesch, “Optimal vaccination strategies for an seir model of infectious diseases with logistic growth,” *Mathematical Biosciences and Engineering* **15**, 485–505 (2018).
- ¹⁸M. H. A. Biswas, L. T. Paiva, and M. de Pinho, “A seir model for control of infectious diseases with constraints,” *Mathematical Biosciences and Engineering* **11**, 761–784 (2014).
- ¹⁹S. Gao, Z. Teng, and D. Xie, “The effects of pulse vaccination on seir model with two time delays,” *Applied Mathematics and Computation* **201**, 282–292 (2008).
- ²⁰J. P. S. M. de Carvalho and A. A. Rodrigues, “Sir model with vaccination: Bifurcation analysis,” *Qualitative Theory of Dynamical Systems* **22** (2023).
- ²¹B. Shulgin, L. Stone, and Z. Agur, “Pulse vaccination strategy in the sir epidemic model,” *Bulletin of Mathematical Biology* **60** (1998).
- ²²J. Duarte, C. Januário, N. Martins, J. M. Seoane, and M. A. F. Sanjuán, “Controlling infectious diseases: The decisive phase effect on a seasonal vaccination strategy,” *International Journal of Bifurcation and Chaos* **31**, 2130044 (2021).
- ²³I. A. Moneim and D. Greenhalgh, “Threshold and stability results for an sirs epidemic model with a general periodic vaccination strategy,” *Journal of Biological Systems* **13**, 131–150 (2005).
- ²⁴I. A. Moneim and D. Greenhalgh, “Use of a periodic vaccination strategy to control the spread of epidemics with seasonally varying contact rate,” *Mathematical Biosciences and Engineering* **2**, 591–611 (2005).
- ²⁵E. C. Gabrick, E. Sayari, P. R. Protachevitz, J. D. S. Jr., K. C. Iarosz, S. L. T. de Souza, A. C. L. Almeida, R. L. Viana, I. L. Caldas, and A. M. Batista, “Unpredictability in seasonal infectious diseases spread,” *Chaos, Solitons and Fractals* **166**, 113001 (2023).
- ²⁶J. A. C. Gallas, “Structure of the parameter space of the hénon map,” *Physical Review Letters* **70**, 2714 (1993).
- ²⁷O. N. Bjørnstad, *Epidemics: Models and Data using R*, 1st ed. (Springer Cham, 2018) pp. XIII, 312.
- ²⁸O. N. Bjørnstad, K. Shea, M. Krzywinski, and N. Altman, “The seirs model for infectious disease dynamics,” *Nature Methods* **17**, 557–558 (2020).
- ²⁹Z. Bai and Y. Zhou, “Global dynamics of an seirs epidemic model with periodic vaccination and seasonal contact rate,” *Nonlinear Analysis: Real World Applications* **13**, 1060–1068 (2012).
- ³⁰E. L. Brugnago, E. C. Gabrick, K. C. Iarosz, J. D. S. Jr., R. L. Viana, A. M. Batista, and I. L. Cadas, “Multistability and chaos in seirs epidemic model with a periodic time-dependent transmission rate,” *Chaos* **33**, 123123 (2023).
- ³¹S. Altizer, A. Dobson, P. Hosseini, P. Hudson, M. Pascual, and P. Rohani, “Seasonality and the dynamics of infectious diseases,” *Ecology Letters* **9**, 467–484 (2006).
- ³²D. J. D. Earn, P. Rohani, B. M. Bolker, and B. T. Grenfell, “A simple model for complex dynamical transitions in epidemics,” *Science* **287**, 667–670 (2000).
- ³³N. C. Grassly and C. Fraser, “Seasonal infectious disease epidemiology,” *Proceedings of the Royal Society* **273**, 2541–2550 (2006).
- ³⁴S. Gao, L. Chen, and Z. Teng, “Analysis of an seirs epidemic model with time delays and pulse vaccination,” *Rocky Moun. Jour. of Math.* **38**, 1385–1402 (2008).
- ³⁵W. E. Boyce and R. C. DiPrima, *Elementary Differential Equations and Boundary Value Problems*, 10th ed. (John Wiley and Sons Ltd, New Jersey, 2012) p. 832.
- ³⁶A. Wolf, J. B. Swift, H. L. Swinney, and J. A. Vastano, “Determining lyapunov exponents from a time series,” *Physica D* **16**, 285–317 (1985).
- ³⁷C. Grebogi, E. Ott, and J. A. Yorke, “Crises, sudden changes in chaotic attractors, and transient chaos,” *Physica D: Nonlinear Phenomena* **7**, 181–200 (1983).
- ³⁸J. A. Gallas, “Dissecting shrimps: results for some one-dimensional physical models,” *Physica A: Statistical Mechanics and its Applications* **202**, 196–223 (1994).
- ³⁹L. C. Martins and J. A. C. Gallas, “Multistability, phase diagrams and statistical properties of the kicked rotor: a map with many coexisting attractors,” *International Journal of Bifurcation and Chaos* **18**, 1705–1717 (2008).
- ⁴⁰J. A. C. Gallas, “Degenerate routes to chaos,” *Physical Review E* **48**, R4156(R) (1993).
- ⁴¹P. C. Rech, “How to embed shrimps in parameter planes of the lorenz system,” *Physica Scripta* **92**, 045201 (2017).
- ⁴²E. S. Medeiros, I. L. Caldas, M. S. Baptista, and U. Feudel, “Trapping phenomenon attenuates the consequences of tipping points for limit cycles,” *Scientific Reports* **7**, 42351 (2017).
- ⁴³U. Feudel, C. Grebogi, B. R. Hunt, and J. A. Yorke, “Map with more than 100 coexisting low-period periodic attractors,” *Physical Review E* **54**, 71–81 (1996).
- ⁴⁴U. Feudel, “Complex dynamics in multistable systems,” *International Journal of Bifurcation and Chaos* **18**, 1607–1626 (2008).
- ⁴⁵C. Grebogi, S. W. McDonald, E. Ott, and J. A. Yorke, “Final state sensitivity: an obstruction to predictability,” *Physics Letters A* **99A**, 415–418 (1983).
- ⁴⁶G. Li, Y. Yue, J. Xie, and C. Grebogi, “Multistability in a quasiperiodically forced piecewise smooth dynamical system,” *Communications in Nonlinear Science and Numerical Simulation* **84**, 105165 (2020).
- ⁴⁷Y.-C. Lai and C. Grebogi, “Quasiperiodicity and suppression of multistability in nonlinear dynamical systems,” *The European Physical Journal Special Topics* **226**, 1703–1719 (2017).
- ⁴⁸M. S. T. de Freitas, R. L. Viana, and C. Grebogi, “Multistability, basin boundary structure, and chaotic behavior in a suspension bridge model,” *International Journal of Bifurcation and Chaos* **14**, 927–950 (2004).
- ⁴⁹P. J. Menck, J. Heitzig, N. Marwan, and J. Kurths, “How basin stability complements the linear-stability paradigm,” *Nature Physics* **9**, 89–92 (2013).
- ⁵⁰U. Feudel and C. Grebogi, “Multistability and the control of complexity,” *Chaos* **7**, 597–604 (1997).
- ⁵¹A. N. Pisarchik and U. Feudel, “Control of multistability,” *Physics Reports* **540**, 167–218 (2014).
- ⁵²B. K. Goswamy and A. N. Pisarchik, “Controlling multistability by small periodic perturbation,” *International Journal of Bifurcation and Chaos* **18**, 1645–1673 (2008).
- ⁵³U. Feudel and C. Grebogi, “Why are chaotic attractors rare in multistable systems?” *Physical Review Letters* **91**, 134102 (2003).